




On Feasibility of Population Inversion Between the Quantum Confinement Levels in Quantum Wells Under Interband Photoexcitation

S. V. Egorov¹ · A. G. Petrov² · A. N. Baranov³ · A. O. Zakhar'in² ·
A. V. Andrianov² 

Received: 27 November 2020 / Accepted: 13 October 2021 / Published online: 1 November 2021
© The Author(s), under exclusive licence to Springer Science+Business Media, LLC, part of Springer Nature 2021

Abstract

We discuss a possibility of achieving population inversion and the associated generation of stimulated terahertz radiation employing transitions between the quantum confinement energy levels of electrons in GaAs/AlGaAs quantum wells under interband photoexcitation. The population inversion occurs between two bottom levels in the conduction band according to a four-level scheme under nonstationary conditions during excitation of electrons from valence band to the top electron state and rapid population of the lower energy level due to processes with the emission of LO-phonons. The time of the depletion of this level due to relatively slow downward energy transitions with the emission of acoustic phonons determines the time interval for the existence of the population inversion, which can amount up to several hundred picoseconds. During this time, the generation of stimulated terahertz radiation is possible at transitions between the two bottom energy levels of electrons in the quantum well.

Keywords Terahertz radiation · Quantum wells · Interband photoexcitation

1 Introduction

Electromagnetic waves of the terahertz spectral range (with frequencies from 0.1 to 10 THz) have been intensively studied for the past three decades. The interest

✉ A. V. Andrianov
alex.andrianov@mail.ioffe.ru

¹ Admiral Makarov State University of Maritime and Inland Shipping,
St. Petersburg, 198035, Russia

² Ioffe Institute, St. Petersburg, 194021, Russia

³ IES, Montpellier University, CNRS, Montpellier, France

in terahertz (THz) radiation stems from the prospects for its application for solving numerous diagnostic tasks in various fields of science and technology. One of the most vexed problems in the use of THz technologies remains the problem of radiation sources. Therefore, studies aimed at creating THz emitters of various types continue to remain extremely relevant [1]. At the beginning of the 2000s, the first electrically pumped THz quantum cascade lasers (QCLs) [2, 3] were demonstrated, the generation of radiation in which arises during intersubband optical transitions of nonequilibrium carriers in structures with multiple quantum wells. Currently, QCLs have been created that can operate at many frequencies of the THz spectral range and have a sufficiently high radiation power [4, 5]. However, THz QCL structures require an extremely complex technology of epitaxial growth and processing, and so far only a few laboratories in the world have mastered this technology. Simpler THz radiation sources are also required for numerous practical applications. An interesting principle of generation of mid-IR laser radiation (with wavelengths of 14–15 μm) due to intersubband transitions of two-dimensional electrons in modulated doped, asymmetric tunnel-coupled GaAs/AlGaAs quantum wells with intraband photoexcitation using a CO₂-laser was demonstrated in Ref. [6, 7] (quantum fountain laser (QFL) based on intersubband transitions [7]). In such QFL structures, a three-level lasing scheme was used with a rapid depletion of the lower laser level due to the emission of polar optical phonons by electrons. Unfortunately, these works [6, 7] did not receive a continuation in the THz spectral region and were only an episode against the background of intensive studies of quantum cascade structures with electrical excitation. Nevertheless, the possibilities of achieving THz lasing on intersubband transitions in quantum wells (QWs) under conditions of optical excitation and in a situation of effective depletion or population of certain laser levels due to processes with the emission of optical phonons are far from being exhausted and are of undoubted practical interest.

In this work, we show that in the most ordinary undoped QWs obtained, for example, in a system of AlGaAs materials, in which the energy gap between the third and second levels of electron quantum confinement (QC) coincides with the LO-phonon energy (36 meV for GaAs), and the gap between the second and first levels is smaller and corresponds to the middle of the THz energy range; under conditions of interband photoexcitation of electrons from the valence band to the third quantum confinement level in the conduction band, population inversion and, accordingly, THz lasing can be achieved.

The paper is organized as follows. Section 2 discusses the details of a model structure with GaAs/AlGaAs quantum wells, in which the energy arrangement of the QC electron subbands corresponds to that mentioned above. The scheme of excitation of electrons to the bottom of the third QC subband from states in the valence band is also discussed here. Section 3 considers the conditions for the formation of a population inversion between the second and first QC energy levels at interband photoexcitation of a QW under the stationary and nonstationary cases. It is shown that, under nonstationary conditions, there should be a population inversion between the second and first QC levels in the QW. Section 4 summarizes the results of the paper. Appendices present results of quantum-mechanical calculations of the characteristic energy relaxation times (relaxation frequencies) of electrons between the QC levels in the QW, the values of which are used as parameters in the basic formulas of Sections 3.

2 Model Structure with GaAs/AlGaAs Quantum Wells

The structures with QWs were selected in such a way as to provide the required energy arrangement of the electron levels in the conduction band and interband photoexcitation using available semiconductor lasers. A structure with undoped GaAs/Al_{0.16}Ga_{0.84}As QWs 23.5 nm wide, with potential well depths at $T = 0$ K for electrons and holes equal to 150 and 73.5 meV, respectively, is suitable for such a task (the values of the band gap of the solid alloy and the conduction and valence band discontinuities for the GaAs/AlGaAs heterojunction were chosen in accordance with the published data [8, 9]). The widths of the barriers in such a structure were assumed to be equal to the widths of the quantum wells (i.e., without tunneling coupling between the wells). The calculations of the energy levels of electrons and holes, as well as their wave functions, in this QW, were carried out using the technique described in Ref. [10]. The quantum well has 4 electronic levels with energies measured from the bottom of the GaAs conduction band, equal to 7.5, 29.6, 65.6, and 113 meV, respectively (Fig. 1). As can be seen, the gap between the second and third quantum confinement levels is 36 meV and corresponds to the LO-phonon energy in GaAs [8]. The three lower energy levels of electrons in the QW are designated as e0,

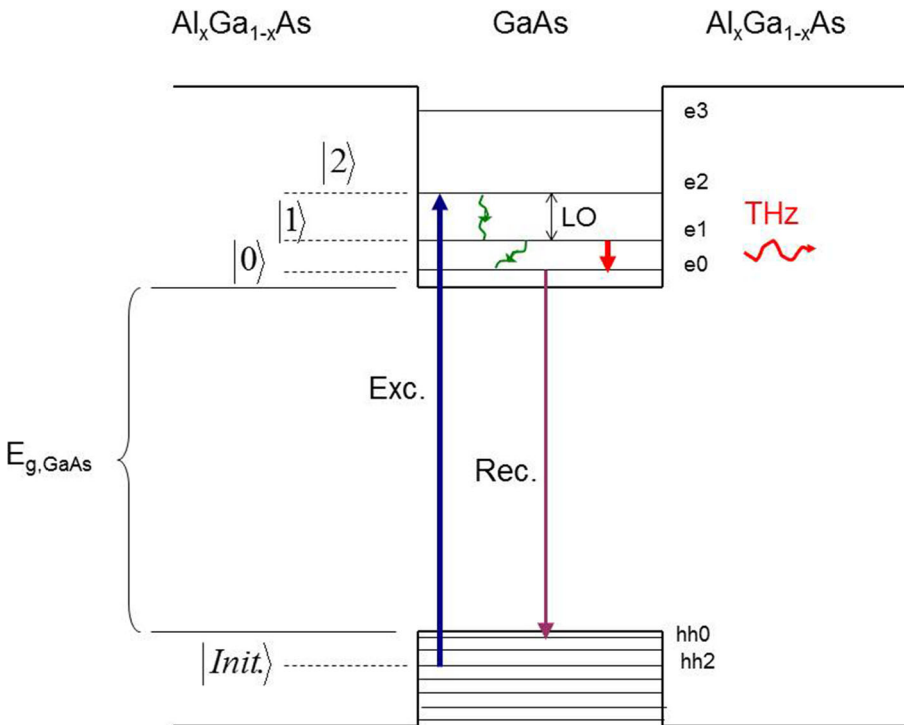


Fig. 1 GaAs/Al_{0.16}Ga_{0.84}As quantum well with a width of 23.5 nm under conditions of excitation of electrons to the third QC level in the conduction band. The states |Init.), |0), |1) and |2) form a four-level THz lasing scheme discussed in this paper. By state |Init.) we mean the initial state in the hh2 → e2 optical transition

e1, and e2 in the diagram shown in Fig. 1. This numbering of the states of electrons is due to the convenience of their parity classification, used in microscopic calculations (see Appendixes (A–E)). This QW has 7 quantum confinement levels for heavy holes with energies measured from the top of the GaAs valence band equal to 1.5, 5.9, 13.3, 24.6, 36.6, 52.0 and 68.6 meV, respectively. Taking this into account, the energy of the interband pumping quantum required for the excitation of electrons to the third QC level, e2, from the states of heavy holes, hh2, in the valence band (see Fig. 1) should be 1.5983 eV at helium temperatures (the corresponding emission wavelength is 775.6 nm).

3 Population Inversion Between Electron Energy Levels in a Quantum Well During Interband Photoexcitation

Let us consider the rate equations for electron populations of quantum confinement levels in a quantum well. We introduce the Fermi electron distribution function $f_n(\mathbf{k}, t)$ in the QC subband with number n and the wave vector \mathbf{k} at the moment of time t . Due to the invariance of the system with respect to rotations in the QW plane, we choose $\mathbf{k} = (k, 0)$, where k is the absolute value of the wave vector. We denote by the symbol $g(k, t)$ the function of generating electrons at the third QC level ($n = 2$). Taking into account the Pauli exclusion principle for transitions between electronic states, the following equations can be written:

$$\frac{\partial f_2(k, t)}{\partial t} = g(k, t) - f_2(k, t) \left\{ [1 - f_1(k, t)] \gamma_{21}^{\text{PO}} + [1 - f_0(\sqrt{2m^*(E_2 - E_0 - \hbar\Omega) + k^2}, t)] \gamma_{20}^{\text{PO}} \right\} \tag{1}$$

$$\frac{\partial f_1(k, t)}{\partial t} = f_2(k, t) [1 - f_1(k, t)] \gamma_{21}^{\text{PO}} - f_1(k, t) \left\{ \Gamma^{\text{IS}} \times [1 - f_0(k, t)] + \iint d\mathbf{k}' [1 - f_0(k', t)] \gamma_{10}^{\text{DA}}(\mathbf{k}, \mathbf{k}') \right\} \tag{2}$$

$$\begin{aligned} \frac{\partial f_0(k, t)}{\partial t} = & -f_0(k) f_{\text{hh0}}(k', t) \Gamma^{\text{IB}} + [1 - f_0(k, t)] \left\{ \gamma_{20}^{\text{PO}} \times \right. \\ & \times \iint f_2(k', t) \delta \left(E_2 + \frac{\mathbf{k}'^2}{2m^*} - E_0 - \frac{\mathbf{k}^2}{2m^*} - \hbar\Omega \right) d\mathbf{k}' + \\ & + \iint f_1(k', t) \gamma_{10}^{\text{DA}}(\mathbf{k}, \mathbf{k}') d\mathbf{k}' + f_1(k, t) \Gamma^{\text{IS}} + \\ & + \left. \iint f_0(k', t) \gamma_{00}^{\text{DA}}(\mathbf{k}, \mathbf{k}') d\mathbf{k}' \right\} - \\ & - f_0(k) \iint [1 - f_0(k', t)] \gamma_{00}^{\text{DA}}(\mathbf{k}, \mathbf{k}') d\mathbf{k}' \end{aligned} \tag{3}$$

here Ω is the optical phonon frequency, m^* is the effective mass of an electron, E_2, E_1, E_0 are the energies of three QC levels in the QW. Two negative terms

in Eq. (1) describe transitions between subbands with emission of polar optical phonon, and γ_{21}^{PO} , γ_{20}^{PO} are the frequencies (probabilities per unit time) of transitions between subbands e2 and e1, e2 and e0, respectively (see Appendix A). The QW parameters are selected in such a way that the e2 \rightarrow e1 transition with the emission of optical phonon is vertical, that is, without changing the electron wave vectors. Equation (2) includes a positive term associated with vertical transitions from the e2 subband, and a negative term associated with transitions from the e1 subband with the emission of acoustic phonons; the probability of such transitions is taken into account by the parameter γ_{10}^{DA} (see Appendix B). In addition, Eq. (2) also includes a negative term associated with optical transitions between subbands e1 and e0, with probability Γ^{IS} (see Appendix E). The first term in Eq. (3) corresponds to interband radiative recombination and, accordingly, contains the factors $f_{\text{hh0}}(k, t) = 1 - f_e^{\text{VB}}(k, t)$ (we neglect the contribution of processes involving light holes to the interband recombination) and the recombination probability Γ^{IB} (see Appendix D). The second, third and fourth terms in this equation describe the influx of electrons from the e2 and e1 subbands due to the emission of phonons and intersubband e1 \rightarrow e0 optical transitions, and the fifth and sixth terms correspond to electron energy relaxation in the lower subband e0 (the parameter γ_{00}^{DA} corresponds to the probability of such processes). In Eqs. (3) and (2), we neglect the interband recombination of electrons from the e2 and e1 subbands because the probability of such a recombination (see Appendix D) is small compared to the probability of intersubband relaxation. We also neglect electron-electron scattering everywhere. It was shown in [11] for the similar system that, for an electron concentration not exceeding $2 \times 10^{11} \text{cm}^{-2}$, electron-electron scattering can be neglected. In our linear theory, the total carrier concentration is naturally proportional to the pumping intensity and this restricts the applicability of our model in the high pump intensity regime.

We consider the system at low temperatures (close to zero temperatures). The applicability of this approximation is not obvious even for temperatures close to the temperature of liquid helium, since optical excitation leads to heating of the electron subsystem. However, since electron-hole pairs are created by interband pumping with an energy close to the threshold energy $\hbar\omega \approx E_G + E_2 + E_{\text{hh2}}$, the heating of electrons in the e2 subband can be considered insignificant, and it can be assumed that $f_1(k, t) = \Theta(k_n^{\text{F}} - |k|)$, where Θ is the Heaviside function, k_n^{F} is rather small the wave vector corresponding to the quasi Fermi level. The parameters of the quantum well are chosen in such a way that $E_{e2} - E_{e1} = \hbar\Omega$, and, therefore, the transitions from the e2 subband to the e1 subband proceed almost exclusively without changing the longitudinal momentum of the electron. Therefore, the distribution function f_1 is similar to f_2 .

For the e0 subband, the heating of electrons cannot be considered small, but such electrons can be conditionally divided into a group of hot and cold.

Let us integrate (1)–(2) over the wave vector in the QW plane. Integration of the distribution function gives the electron concentration. For the e2 and e1 subbands, all electrons are concentrated in the region of small wave vectors. Consequently, it

is possible to introduce the electron concentrations in the subbands, $n_2(t)$ and $n_1(t)$, respectively. For the terms associated with vertical transitions, we get:

$$\begin{aligned} & \frac{1}{4\pi^2} \iint f_2(k, t) [1 - f_1(k, t)] d\mathbf{k} \\ &= \frac{1}{\pi} \int_0^\infty \Theta(k_2^F - |k|) \left[1 - \Theta(k_1^F - |k|) \right] k dk = n_2 - n_1, \end{aligned} \tag{4}$$

This equation reflects the fact that the transitions from the bottom of the e2 subband to the bottom of the e1 subband are forbidden by the Pauli principle and only electrons located in the phase space in the $k_2^F > k > k_1^F$ ring make the main contribution to the transitions. Integration of the term responsible for interband radiative recombination gives:

$$\begin{aligned} & \frac{1}{4\pi^2} \iint d\mathbf{k} f_0(k, t) f_{hh0}(k, t) \\ &= \frac{1}{\pi} \int_0^\infty \Theta(k_0^F - |k|) \Theta(k_{hh0}^F - |k|) k dk = \min(n_0, p_0) = n_0(t) \end{aligned} \tag{5}$$

here, the high rate of intraband energy relaxation of heavy holes and the property of electroneutrality are taken into account: $p_0 = n_2 + n_1 + n_0 + \tilde{n}_0$, where \tilde{n}_0 is the concentration of hot electrons, and n_0 is the concentration of cold electrons, that is, those located at the bottom of the subband e0 and participating in interband recombination.

As a result of performing this integration, from Eqs. (1)–(3), one can go to the following system of balance equations for the electron concentrations in the subbands of the quantum well:

$$\frac{\partial n_2(t)}{\partial t} = G(t) - [n_2(t) - n_1(t)] \Theta(n_2(t) - n_1(t)) \gamma_{21}^{PO} - n_2(t) \gamma_{20}^{PO} \tag{6}$$

$$\begin{aligned} \frac{\partial n_1(t)}{\partial t} &= [n_2(t) - n_1(t)] \Theta(n_2(t) - n_1(t)) \gamma_{21}^{PO} - \\ & - n_1(t) \gamma_{10}^{DA} - \Gamma^{IS} [n_1(t) - n_0(t)] \Theta(n_1(t) - n_0(t)) \end{aligned} \tag{7}$$

$$\begin{aligned} \frac{\partial n_0(t)}{\partial t} &= n_2(t - T) \gamma_{20}^{PO} + n_1(t - T) \gamma_{10}^{DA} - \Gamma^{IB} n_0(t) + \\ & + \Gamma^{IS} [n_1(t) - n_0(t)] \end{aligned} \tag{8}$$

$$\tilde{n}_0(t) = \int_{t-T}^t \left[n_2(t) \gamma_{21}^{PO} + n_1(t) \gamma_{10}^{DA} \right] dt \tag{9}$$

where $G(t)$ is the rate of generation of electrons by light. Despite the fact that $f_0(k, t) \ll 1$ for $k > k_0^F$, $\tilde{n}_0(t)$ is obtained by integration over a significant volume of the phase space and, generally speaking, will not be small. As discussed in Appendixes B and C, upon transitions from the e1 subband to the e0 subband, the transfer of a small wave vector to acoustic phonon in the QW plane (q_{\parallel}) is unlikely. The main transitions in such an energy relaxation occur when the electron energy changes in small portions with the transfer of sizeable wave vectors to the phonons. Figure 2 schematically shows the process of energy relaxation into the e0 subband

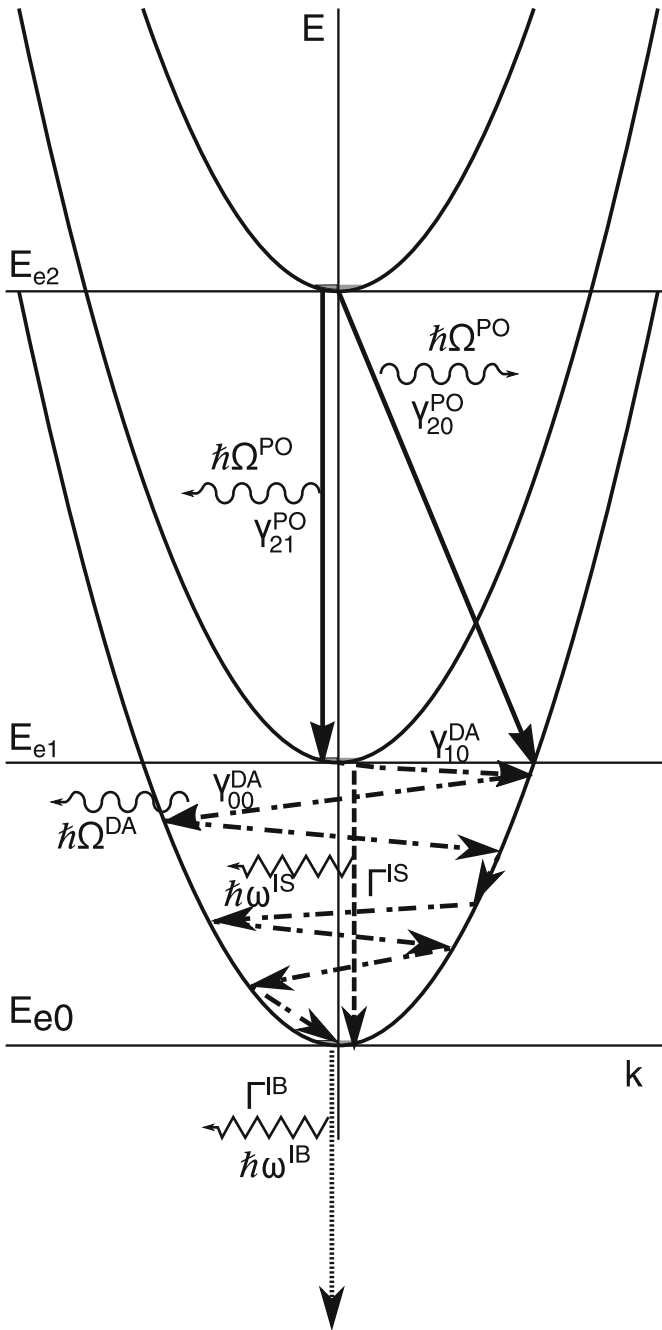


Fig. 2 Scheme of electron transitions in the process of energy relaxation to the quantum confinement subband e_0 . Solid arrows correspond to transitions with emission of optical phonons. Dash-dotted arrows correspond to transitions with emission of acoustic phonons during relaxation between the subbands e_1 and e_0

with the emission of phonons. Strictly speaking, $f_0(k, t)$ should be obtained by solving the Boltzmann kinetic equation for electrons. However, instead of this we use the average rate of energy loss (see Appendix C) in order to take into account the finite relaxation time of electrons on acoustic phonons in the lowest subband through the “delay” time:

$$T = \int_{E_{\min}}^{E_1 - E_0} \left(\frac{dE}{dt} \right)^{-1} dE. \quad (10)$$

where E_{\min} is the characteristic kinetic energy of motion in the QW plane, separating the region of hot (energy-relaxing) and cold electrons (calculations show that $E_{\min} \approx \frac{\hbar^2}{2m^*} \left(\frac{1}{a} \right)^2 \approx 1$ meV). Calculating the time T according to Eq. (10) gives a value of the order of 6×10^{-10} s. Equations (8)–(9) in the system of balance equations are written taking into account such “delay” time.

We will assume that the photoexcitation in time has the shape of a step, that is $G(t) = G\Theta(t)$. The solutions of the system of Eqs. (6)–(9) for the electron concentration in the QC subbands as a function of time with zero initial conditions in this case will have the following form:

$$n_2(t) = \frac{G}{\gamma_+ \gamma_-} \left\{ \gamma_{21}^{\text{PO}} + \gamma_{10}^{\text{DA}} - \frac{\gamma_{10}^{\text{DA}} \gamma_2 + \tilde{\gamma}^2 - \gamma_{21}^{\text{PO}} \gamma_-}{2\gamma_2} e^{-\gamma_+ t} - \frac{\gamma_{10}^{\text{DA}} \gamma_2 - \tilde{\gamma}^2 + \gamma_{21}^{\text{PO}} \gamma_+}{2\gamma_2} e^{-\gamma_- t} \right\} \quad (11)$$

$$n_1(t) = \frac{G \gamma_{21}^{\text{PO}}}{\gamma_+ \gamma_-} \left\{ 1 - \frac{\gamma_+}{2\gamma_2} e^{-\gamma_- t} + \frac{\gamma_-}{2\gamma_2} e^{-\gamma_+ t} \right\} \quad (12)$$

$$n_0(t) = G \frac{\gamma_{21}^{\text{PO}} \Gamma^{\text{IS}}}{\gamma_+ \gamma_-} \left[t - \frac{\gamma_+}{2\gamma_2 \gamma_-} (1 - e^{-\gamma_- t}) + \frac{\gamma_-}{2\gamma_2 \gamma_+} (1 - e^{-\gamma_+ t}) \right] \quad \text{at } 0 \leq t < T \quad (13)$$

$$n_0(t) = G \left\{ \frac{1 - e^{-(t-T)\gamma_+}}{\Gamma^{\text{IB}}} + \frac{\gamma_+ - \gamma_{20}^{\text{PO}}}{\gamma_-} e^{-(t-T)\gamma_-} + \frac{\gamma_{20}^{\text{PO}} - \gamma_-}{\gamma_+} e^{-(t-T)\gamma_+} \right\} \quad \text{at } t > T \quad (14)$$

$$\tilde{n}_0(t) = G \left\{ t + \frac{2\gamma_{21}^{\text{PO}} + \gamma_{10}^{\text{DA}}}{\gamma_+ \gamma_-} + \frac{\gamma_{20}^{\text{PO}} - \gamma_-}{2\gamma_2 \gamma_-} e^{-\gamma_+ t} + \frac{\gamma_+ - \gamma_{20}^{\text{PO}}}{2\gamma_2 \gamma_+} e^{-\gamma_- t} \right\} \quad \text{at } 0 \leq t < T \quad (15)$$

$$\tilde{n}_0(t) = GT \quad \text{at } t > T \quad (16)$$

here $\gamma_{\pm} = \gamma_{21}^{\text{PO}} + \frac{\gamma_{20}^{\text{PO}} + \gamma_{10}^{\text{DA}}}{2} \pm \gamma_2$, $\gamma_2 = \sqrt{(\gamma_{21}^{\text{PO}})^2 + \frac{(\gamma_{20}^{\text{PO}})^2 - \gamma_{10}^{\text{DA}}(2\gamma_{20}^{\text{PO}} - \gamma_{10}^{\text{DA}})}{4}}$, $\tilde{\gamma} = \sqrt{\gamma_{21}^{\text{PO}}\gamma_{20}^{\text{PO}} + \frac{\gamma_{10}^{\text{DA}}}{2}(\gamma_{20}^{\text{PO}} - \gamma_{10}^{\text{DA}})}$. The numerical values of the characteristic frequencies γ_{21}^{PO} , γ_{20}^{PO} , γ_{10}^{DA} , Γ^{IS} and Γ^{IB} for the system under consideration are calculated in Appendixes A–E and are 7.3×10^{11} , 1.2×10^{11} , 2.6×10^{10} , 1.1×10^6 and $\approx 2.8 \times 10^8 \text{ s}^{-1}$, respectively. Taking this into account, the frequency values γ_2 , $\tilde{\gamma}$, γ_+ and γ_- are about 7.3×10^{11} , 3×10^{11} , 1.5×10^{12} and $7.3 \times 10^{10} \text{ s}^{-1}$, respectively.

The results of calculations according to Eqs. (11)–(16) of the time dependence of the electron concentrations at the QC levels, normalized to the value of GT , are shown in Fig. 3.

As can be seen under nonstationary conditions, at times shorter than about 600 ps, there is a population inversion between the second and first electron QC levels in given QW. Figure 3 also shows that the strongly coupled states e1 and e2 are separated from the ground state e0, the transitions to which are hindered. It is clear that the time interval of inversion existence of $\approx 0\text{--}600 \text{ ps}$ is mainly determined by the time of slow relaxation of nonequilibrium electrons in the e0 subband with the emission of acoustic phonons at low energy losses in individual phonon emission events.

The results of solving the system of Eqs. (11)–(16) at times significantly longer than the time T are shown in Fig. 4. It is seen that under these conditions there is no population inversion in the system.

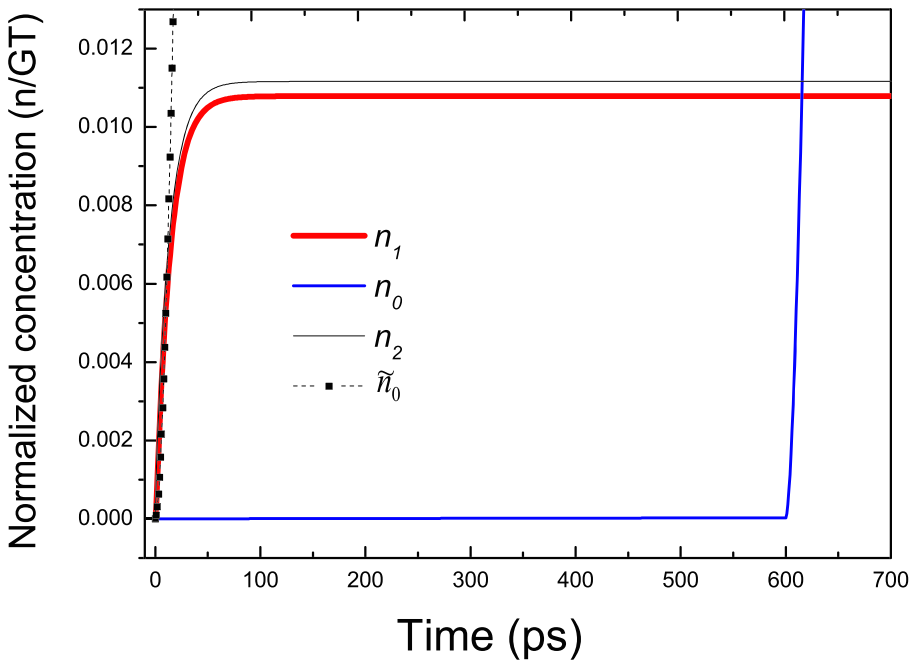


Fig. 3 Time dependence of the normalized populations of the third, second and first electron QC levels in QW (e2, e1 and e0, respectively) under interband photoexcitation

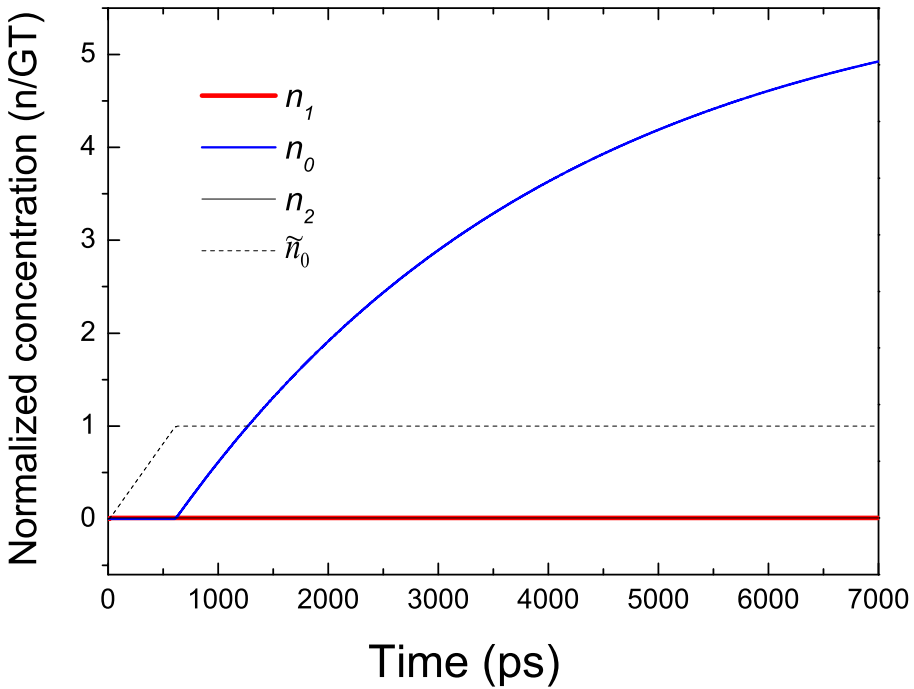


Fig. 4 Time dependence of the normalized electron concentrations in the QW subbands at large times.

Stationary values of the electron concentration in the QC subbands can also be obtained from Eqs. (11)–(16) in the limit of $t \rightarrow \infty$. Considering that $\gamma_{21}^{PO}, \gamma_{20}^{PO} \gg \gamma_{10}^{DA}$, we get the following:

$$\begin{aligned} \lim_{t \rightarrow \infty} n_2(t) &= G \frac{\gamma_{20}^{PO} + \gamma_{21}^{PO}}{\gamma_+ \gamma_-} \approx G \left(\frac{1}{\gamma_{20}^{PO}} + \frac{1}{\gamma_{21}^{PO}} \right) + \\ &+ G \gamma_{10}^{DA} \left(\frac{1}{\gamma_{20}^{PO}} + \frac{1}{\gamma_{21}^{PO}} \right)^2 + o \left(\frac{\gamma_{10}^{DA}}{\gamma_{21}^{PO}} \right) \end{aligned} \tag{17}$$

$$\begin{aligned} \lim_{t \rightarrow \infty} n_1(t) &= G \frac{\gamma_{21}^{PO}}{\gamma_+ \gamma_-} \approx \frac{G}{\gamma_{20}^{PO}} \left\{ 1 - \right. \\ &\left. - \gamma_{10}^{DA} \left(\frac{1}{\gamma_{20}^{PO}} + \frac{1}{\gamma_{20}^{PO}} \right) \right\} + o \left(\frac{\gamma_{10}^{DA}}{\gamma_{21}^{PO}} \right) \end{aligned} \tag{18}$$

$$\lim_{t \rightarrow \infty} n_0(t) = \frac{G}{\Gamma_{IB}} \tag{19}$$

$$\lim_{t \rightarrow \infty} \tilde{n}_0(t) = GT \tag{20}$$

It can be seen from Eqs. (18)–(19) that the stationary population inversion, which could potentially lead to the generation of stimulated THz radiation at the

transitions between the second and first QC levels, would mean that the following takes place:

$$\Gamma^{\text{IB}} > \gamma_{20}^{\text{PO}}, \quad (21)$$

that is, the probability of depletion of the $e0$ level due to interband recombination (in our case, this is spontaneous interband recombination) should be higher than the probability of intraband transitions, which cannot be achieved under normal conditions.

It should be noted that in the case of the appearance of stimulated interband optical transitions from the state $e0$, the frequency Γ^{IB} can significantly increase and the inequality (21) can in principle be fulfilled. Interestingly, the idea of simultaneous laser generation of radiation on intraband and interband optical transitions in quantum wells was put forward in Ref. [12].

Thus, under the conditions of nonstationary interband photoexcitation of electrons to the third quantum confinement level, a population inversion arises between the second and first QC levels in this QW. In such a situation, the appearance of stimulated THz radiation on the $e1 \rightarrow e0$ transitions with a quantum energy of the order of 22.1 meV is quite possible. This THz radiation should be linearly polarized along the growth axis of the structure with QWs [10] and will propagate predominantly along layers with QWs. A THz laser resonator in such structures can be created by simply cleaving the crystal along the cleavage planes.

The considered scheme for creating a population inversion (Fig. 1) is somewhat simplified. In reality, at the selected energy of the photoexcitation, along with the “useful” photogeneration of electrons from the heavy holes states to the bottom of the third QC subband ($e2$) in the conduction band, there will also be a “parasitic” photoexcitation of electrons into the first and second QC subbands ($e0$ and $e1$, respectively) to the states with large wave vectors in the QW plane. But population of the lower subband with hot electrons due to transitions $hh0 \rightarrow e0$ at large k will simply lead to an increase in the number of electrons in the region of large k in the $e0$ subband. Strictly speaking, to take into account such transitions, it is necessary to add the corresponding terms to the balance equation. However, even in the worst scenario, if we neglect the reverse transitions from $e0$ to $e1$, which are beneficial to us and will only increase the effect we have proposed, we will only increase the number of hot electrons in the main subband, while the critically important for us is the low concentration of cold electrons in the main subband during time T . Our estimates show that the results will not change qualitatively. The transitions $hh1 \rightarrow e1$ will also not change the main results, since taking such transitions into account will lead to an increase in the number of electrons in the $e1$ subband and thereby increase the effect of population inversion between the subbands.

For the chosen energy of the photoexcitation, transitions from the subbands of light holes will also take place. These are $lh1 \rightarrow e1$ and $lh0 \rightarrow e0$ transitions. Transitions of $lh2 \rightarrow e2$ type are not possible due to the chosen pump quantum energy. During the $lh1 \rightarrow e1$ transitions, nonequilibrium electrons are created in the second QC subband and, in principle, give a positive contribution to the formation of population inversion between the levels in the quantum well according to the mechanism considered in this paper. As a result of the $lh0 \rightarrow e0$ transitions, electrons are also generated in $e0$ subband in states with large k vectors in the QW plane, and taking

them into account will only slightly (the square of the matrix element of the interband transition from the heavy holes state is three times larger than from the light holes state for light directed along the z -axis [16]) increase the number of hot electrons in the main subband, slowly (over time of order of T) relaxing downward in energy. Estimates show that taking into account such additional hot electrons also does not quantitatively change the result obtained. In addition, the probability of light absorption in transitions involving light holes is three times lower than that involving heavy holes. Therefore, the photogeneration of electrons from the subbands of light holes can also be neglected.

In a real situation, in structures with GaAs/Al $_x$ Ga $_{1-x}$ As quantum wells, there will be fluctuations in both the widths of the quantum wells and the concentration of Al in the barriers. The estimates show that with a fluctuation in the QW width of the order of 1 monolayer and a fluctuation in the Al content of the order of 1% (such values are quite real for modern setups for molecular beam epitaxy in the AlGaAs system), the corrections to the energy gaps between the electron QC levels in the considered QWs will be less than 1 meV. Therefore, the influence of the effects of fluctuation of the composition of the solid alloy and the width of the QW in our problem can also be neglected.

The generation of nonequilibrium carriers with high densities in quantum wells will lead to a change in the position of the electron QC levels due to the Coulomb and exchange-correlation interaction between the carriers [17, 18]. Estimations of the influence of these effects (see Appendixes F and G) show that for the concentrations of nonequilibrium carriers considered in our task no higher than $2 \times 10^{11} \text{cm}^{-2}$, the corrections to the values of the energy gaps between the QC levels will be no more than 0.6 meV. Such corrections are insignificant and cannot considerably change the main result of our paper.

Nonequilibrium carriers will have the strongest influence on the value of the band gap due to the effect of band gap renormalization (BGR) [17, 18]. It is estimated that the change in the band gap width can reach tens of meV at the maximum concentrations of nonequilibrium carriers of the order of $2 \times 10^{11} \text{cm}^{-2}$ considered in our paper. But since the effect considered in our paper is more of a threshold than a resonant one, the BGR will not have a significant impact on the final result.

4 Summary

In conclusion, we have discussed the possibility of achieving population inversion between the quantum confinement energy levels in undoped GaAs/Al $_{0.16}$ Ga $_{0.84}$ As 23.5 nm wide quantum wells and, accordingly, the generation of stimulated THz radiation under interband photoexcitation. It is shown that, under optical pumping from the valence band to the third QC level in the conduction band, separated from the second QC electron level by the LO-phonon energy, population inversion occurs between the second and first QC levels in the beginning of the excitation pulse. The LO-phonon resonance between upper QC levels provides fast population of the second QC level, while the lowest electron state is populated much more slowly, with a characteristic time of the order of several hundreds of picoseconds controlled by the

energy relaxation processes with the emission of acoustic phonons. Such a system may turn out to be convenient for the development of a new type of THz laser based on intersubband transitions with optical excitation.

Appendix A. Intersubband transitions with emission of polar optical phonons

The problem of intersubband scattering of electrons in a QW has been considered by many authors, beginning with the work of B. K. Ridley [13]. A detailed presentation of the results obtained can be found in Ref. [14]. It was shown (see [14]) that for QWs with widths larger than 10 nm, one can neglect both the quantum confinement of phonons and the interface modes and use the approximation of bulk phonon modes. The matrix elements of the electron-phonon interaction for such a model were presented in Refs. [15, 16]. We are primarily interested in the relaxation of electrons from the bottom of the overlying subbands to the underlying subbands. In the general case, the transition occurs to the electron state with momentum $\hbar\mathbf{k}_{\parallel}$ directed in the plane of the QW. For the transition from the bottom of the subband, the momentum conservation law establishes a connection between the wave vectors of the electron and the phonon participating in the process: $\mathbf{k}_{\parallel} = -\mathbf{q}_{\parallel}$. Using Fermi’s golden rule and summing over the phonon modes, we obtain the following for the probability of transition from state f to state i (i and f take the values 0, 1, 2, ...):

$$w_{fi} = \frac{e^2\Omega}{4\pi\epsilon_c} \int_{-\infty}^{\infty} dq_z |M_{fi}(q_z)|^2 \int_{-\infty}^{\infty} dq_{\parallel} \frac{q_{\parallel}}{q_z^2 + q_{\parallel}^2} \tag{A.1}$$

$$\times \delta(E_f - E_i - \frac{\hbar^2 q_{\parallel}^2}{2m^*} - \hbar\Omega) = \frac{e^2\Omega m^*}{4\pi\epsilon_c \hbar^2} \int_{-\infty}^{\infty} dq_z \frac{|M_{fi}(q_z)|^2}{q_z^2 + q_0^2}$$

where Ω is the frequency of the optical phonon, m^* is the effective mass of the electron, e is the charge of the electron, and $\epsilon_c = (1/\epsilon_{\infty} - 1/\epsilon_0)^{-1}$, here ϵ_{∞} and ϵ_0 are the dynamic and static dielectric permittivity of GaAs, respectively, $q_0 = \sqrt{2m^*(E_f - E_i - \hbar\Omega)}/\hbar$ is the value of the longitudinal (in the QW plane) wave vector obtained by the phonon during scattering from the bottom of the subband; it is equal to the value of the wave vector of the electron in the final state.

A1.1 A Rectangular quantum well of infinite depth

The explicit form of the phonon matrix element $M_{fi}(q_z) = \int_{-\infty}^{\infty} \psi_f^*(z) \exp(iq_z z) \psi_i(z) dz$ depends on the chosen model and will be different in the case of QWs of finite and infinite depth. So, for an infinitely deep QW with a width a , according to Refs. [15, 16], the matrix element can be represented as:

$$M_{fj}(q_z) = \frac{\pi^2 q_z^2 a^2 (\sigma^2 - \delta^2)}{(q_z^2 a^2 - \pi^2 \sigma^2)(q_z^2 a^2 - \pi^2 \delta^2)} \left[e^{\frac{1}{2} q_z a} + (-1)^{\sigma} e^{-\frac{1}{2} q_z a} \right] \tag{A.2}$$

$\sigma = f + j$, $\delta = f - j$, where j and f take the values 0, 1, 2, ... This matrix element has a resonant character and the integral over q_z in Eq. (A.1) can be calculated using the residue theorem. As a result, we get the following:

$$w_{fi} = \frac{e^2 m^* \Omega a}{4\pi \epsilon_c \hbar^2} (\zeta_{i-f, i+f+2} + \zeta_{i+f+2, i-f}), \text{ where} \tag{A.3}$$

$$\zeta_{l,j} = \frac{1 - [1 - (-1)^l e^{-q_0 a}] \left(\frac{4l^2}{(j^2 - l^2) q_0 a} + \frac{2q_0 a}{\pi^2 l^2 + q_0^2 a^2} \right)}{\pi^2 l^2 + q_0^2 a^2}$$

In our case, the transition between the third and second quantum confinement levels ($e2 \rightarrow e1$) is resonant one, that is $q_0 = 0$, $E_2 - E_1 = \hbar\Omega$, $\Omega = \frac{5\hbar\pi^2}{2m^* a^2}$ and from Eq. (A.3) we get: $w_{21} = \frac{13e^2\pi}{10\hbar\epsilon_c a}$. For the

$e2 \rightarrow e0$ transition on the other hand, $q_{20} = \sqrt{3}/a$ and calculations by Eq. (A.3) give the following for the transition probability: $w_{20} \approx \frac{65e^2\pi}{266\hbar\epsilon_c a}$. Accordingly, the ratio of probabilities w_{21}/w_{20} is about 5.3.

A1.2 A rectangular quantum well of finite depth

For a well of finite depth, the following expressions can be obtained for the squares of the phonon matrix elements:

$$|M_{20}(q_z)|^2 = \frac{64\kappa_0\kappa_2k_0^2k_2^2q_z^2 \left\{ [q_z^2 - (\kappa_0 + \kappa_2)^2] \sin \frac{q_z a}{2} - 2q_z(\kappa_0 + \kappa_2) \cos \frac{q_z a}{2} \right\}^2}{(2 + \kappa_0 a)(2 + \kappa_2 a) [(k_0 + k_2)^2 - q_z^2]^2 [(k_0 - k_2)^2 - q_z^2]^2 [(\kappa_0 + \kappa_2)^2 + q_z^2]^2} \tag{A.4}$$

$$|M_{21}(q_z)|^2 = \frac{64\kappa_1\kappa_2k_1^2k_2^2q_z^2 \left\{ [q_z^2 - (\kappa_1 + \kappa_2)^2] \cos \frac{q_z a}{2} + 2q_z(\kappa_1 + \kappa_2) \sin \frac{q_z a}{2} \right\}^2}{(2 + \kappa_1 a)(2 + \kappa_2 a) [(k_1 + k_2)^2 - q_z^2]^2 [(k_1 - k_2)^2 - q_z^2]^2 [(\kappa_1 + \kappa_2)^2 + q_z^2]^2} \tag{A.5}$$

where $k_j = \sqrt{2m^*E_j/\hbar}$ and $\kappa_j = \sqrt{2m^*(U - E_j)/\hbar}$, U is the depth of the potential well. As a result of cumbersome calculations, which we omit, we can obtain the following general expression for the transition probability:

$$w_{fi} = \frac{e^2\Omega}{4Y\epsilon_c a} \left(1 + \frac{2}{\kappa_i a}\right)^{-1} \left(1 + \frac{2}{\kappa_f a}\right)^{-1} \left(E_i + E_f + E_q + \frac{\hbar^2}{2m^*a^2} \left\{ \frac{E_i(3E_f + E_i + E_q)\kappa_f a - E_f(3E_i + E_f + E_q)\kappa_i a}{U(E_i - E_f)} - \frac{8q_0 a E_f E_i}{Y} \left[1 \mp e^{-q_0 a} \left(\frac{\kappa_i + \kappa_f - q_0}{\kappa_i + \kappa_f + q_0} \right)^2 \right] \right\} \right) \tag{A.6}$$

where $Y = 4E_f(E_i - E_f - \hbar\Omega) + (\hbar\Omega)^2$, and $E_q = \frac{\hbar^2 q_0^2}{2m^*}$, the sign \mp corresponds to transitions between states with the same or different parity. From formula (A.6), one can obtain formula (A.3) in the limit of $U \rightarrow \infty$. The expansion of exact formula (A.6) in a series for large U for the two transitions of interest $e2 \rightarrow e1$ and $e2 \rightarrow e0$ has the following form:

$$w_{12} = \frac{13e^2\pi}{10\hbar\epsilon_c a} \left(1 + \frac{\hbar}{a\sqrt{2m^*U}} + \dots \right) \tag{A.7}$$

$$w_{02} = \frac{e^2\pi}{\hbar\epsilon_c a} \left\{ \frac{65}{266} - \frac{360\sqrt{3}}{17689\pi} \left[1 - e^{-\sqrt{3}\pi} \right] \right\} \left(1 + \frac{\hbar}{a\sqrt{2m^*U}} + \dots \right) \tag{A.8}$$

As expected, the corrections to the transition probabilities associated with taking into account the finite depth of the potential well are inversely proportional to the QW power, $\frac{q}{\hbar} \sqrt{2m^*U}$. Note that, as is well known [16], corrections to the energy of deep states in the QW are also inversely proportional to the power of the well. Calculations using Eqs. (A.7) and (A.8) give the probabilities per unit time for transitions with emission of polar optical phonons between states $e2$ and $e1$, $e2$ and $e0$, in the considered quantum well, equal to $w_{21}^{PO} = 7.3 \times 10^{11} s^{-1}$ and $w_{20}^{PO} = 1.2 \times 10^{11} s^{-1}$.

Appendix B. Energy relaxation with the emission of deformation acoustic phonons

For the intersubband ($e1 \rightarrow e0$) and intraband ($e0 \rightarrow e0$) transitions with the emission of acoustic phonons, expressions can be obtained for the squares of phonon matrix elements, which are generally

similar in structure to those given in Eqs. (A.4)–(A.5) and which in this case will have the following form:

$$|M_{10}(q_z)|^2 = \frac{64\kappa_0\kappa_1k_0^2k_1^2q_z^2 \left[[q_z^2 - (\kappa_0 + \kappa_1)^2] \cos \frac{q_z a}{2} + 2q_z(\kappa_0 + \kappa_1) \sin \frac{q_z a}{2} \right]^2}{(2 + \kappa_0 a)(2 + \kappa_1 a) [(k_0 + k_1)^2 - q_z^2]^2 [(k_0 - k_1)^2 - q_z^2]^2 [(\kappa_0 + \kappa_1)^2 + q_z^2]^2} \tag{A.9}$$

$$|M_{00}(q_z)|^2 = \frac{64\kappa_0^2k_0^4 \left\{ [q_z^2 - 4\kappa_0^2] \sin \frac{q_z a}{2} - 4q_z\kappa_0 \cos \frac{q_z a}{2} \right\}^2}{q_z^2(2 + \kappa_0 a)(2 + \kappa_2 a) (4\kappa_0^2 - q_z^2)^2 (4\kappa_0^2 + q_z^2)^2} \tag{A.10}$$

where also $k_j = \sqrt{2m^*E_j/\hbar}$ and $\kappa_j = \sqrt{2m^*(U - E_j)/\hbar}$.

Let us consider transitions from states near the bottom of the second quantum confinement subband (subband e1). In this case, the wave vector of the electron motion in the QW plane in the initial state is $k_{\parallel}=0$. It is clear from the law of conservation of momentum that in the final state (in the subband e0) the wave vector of an electron will be equal in absolute value to the longitudinal (in the QW plane) wave vector of the emitted phonon $k_{0\parallel} = q_{\parallel}$. From the law of energy conservation it follows that:

$$E_1 - E_0 - \frac{\hbar^2 q_{\parallel}^2}{2m^*} = \hbar s_l \sqrt{q_z^2 + q_{\parallel}^2}, \tag{A.11}$$

where s_l is the speed of sound in the longitudinal mode. It is clear from Eq. (A.11) that at $q_{\parallel} \rightarrow 0$ the value of the phonon wave vector q_z in the direction perpendicular to the QW plane tends to q_z^* equal to $\approx \frac{E_1 - E_0}{\hbar s_l}$, and in our case $q_z^* a = 153$. If we take into account that for large q_z the square of the matrix phonon element $M_{10}^2(q_z)$ (see Eq. (A.9)) behaves like $(1/q_z a)^6$, then we can conclude that vertical transitions (with zero q_{\parallel}) between the subbands e1 and e0 practically impossible. Transitions with the emission of acoustic phonons occur when the electron energy changes in small portions with the transfer of sizeable wave vectors to the phonon. The picture of such transitions is shown schematically in Fig. 2.

Unlike relaxation of the electron energy on optical phonons, here at different temperatures not only “zero-point” relaxation (on zero-point lattice vibrations) is possible, but also “equipartition” relaxation [19], when the lattice temperature, expressed in energy units, is of the order of or higher than the characteristic phonon energy. Therefore, in the general case, both processes with emission and processes with absorption of phonons are possible. Despite the fact that the total energy of an electron increases upon absorption of a phonon, the electron passes into another subband, the rate of intraband relaxation along which is usually higher than for intersubband relaxation (within the framework of the same mechanism). Therefore, the next act of emission of a phonon will be more likely within the same subband to which the electron passed as a result of absorption of an acoustic phonon.

The general expression for the probability of intersubband relaxation of the electron energy with the emission of acoustic phonons has the form [19]:

$$w = \frac{\Xi^2}{4\pi\rho s_l} \int_{-\infty}^{\infty} dq_z \int_0^{\infty} dq_{\parallel} (q_z^2 + q_{\parallel}^2) |M_{fi}(q_z)|^2 \tag{A.12}$$

$$\times \left[\frac{\delta \left(\Delta E - \frac{\hbar^2 q_{\parallel}^2}{2m^*} - \hbar s_l \sqrt{q_z^2 + q_{\parallel}^2} \right)}{1 - e^{-\frac{\hbar s_l}{k_B T} \sqrt{q_z^2 + q_{\parallel}^2}}} + \frac{\delta \left(\Delta E - \frac{\hbar^2 q_{\parallel}^2}{2m^*} + \hbar s_l \sqrt{q_z^2 + q_{\parallel}^2} \right)}{e^{\frac{\hbar s_l}{k_B T} \sqrt{q_z^2 + q_{\parallel}^2}} - 1} \right]$$

where Ξ — deformation potential, ρ — material density, k_B — Boltzmann constant. The structure of the squares of the matrix elements $M_{fi}^2(q)$ is given above in expressions (A.10) and (A.9). In the case of high temperatures (say, at $T = 78$ K and higher), “equipartition” relaxation becomes essential, and in this approximation, the following expression can be obtained for the transition probability:

$$w_{EP} = \frac{m^* \Xi^2 k_B T a}{\pi \rho s_l^2 \hbar^3} \int_0^{\infty} \sqrt{q_z^2 + \frac{2m^* \Delta E}{\hbar^2}} |M_{fi}(q_z)|^2 dq_z. \tag{A.13}$$

In the case of low temperatures (say, of the order of $T = 4.2$ K), we can restrict ourselves to only the “zero-point” approximation:

$$w_{ZP} = \frac{m^* \Xi^2 a}{2\pi \rho s_l \hbar^2} \int_0^{\infty} \left(q_z^2 + \frac{2m^* \Delta E}{\hbar^2} \right) |M_{fi}(q_z)|^2 dq_z. \tag{A.14}$$

Calculations according to Eq. (A.14) of the energy relaxation times on acoustic phonons for the quantum wells considered in this article give: $w_{10}^{\text{DA}} = 2.6 \times 10^{10} \text{s}^{-1}$, $w_{21}^{\text{DA}} = 5.1 \times 10^{10} \text{s}^{-1}$, and $w_{20}^{\text{DA}} = 5.1 \times 10^{10} \text{s}^{-1}$.

Appendix C. Intraband energy relaxation

The most efficient mechanism of energy relaxation on acoustic phonons is the emission of a large number of low-energy phonons. This allows us to introduce the average rate of energy loss by electrons [20]:

$$\left\langle \frac{dE(k)}{dt} \right\rangle = \hbar s_l \sum_{\mathbf{q}} |\mathbf{q}| w(\mathbf{q}), \quad (\text{A.15})$$

where $w(\mathbf{q})$ is the probability of emission of an acoustic phonon with a wave vector \mathbf{q} by an electron. For the process of energy relaxation in the e_0 subband with a predominance of “zero-point” relaxation, the following can be obtained:

$$\left\langle \frac{dE(k)}{dt} \right\rangle_{\text{ZP}} = \frac{m^* \Xi^2 a}{4\pi \rho \hbar} \int_0^\infty \left(q_z^2 + \frac{2m^* \Delta E}{\hbar^2} \right)^{3/2} |M_{00}(q_z)|^2 dq_z. \quad (\text{A.16})$$

In the approximation of $ka > 1$, from Eq. (A.16) one can obtain the following expression for the rate of electron energy losses:

$$\left\langle \frac{dE(k)}{dt} \right\rangle_{\text{ZP}} \approx \frac{8\pi m^* \Xi^2}{\rho \hbar} \left[k^3 + \frac{3k\pi^2}{4a^2} + \frac{3\pi^4}{ka^4} \left(1 + 2 \ln \frac{4ka}{\pi} \right) \right] + o\left(\frac{1}{ka}\right) \quad (\text{A.17})$$

From expression (A.17) it can be seen that the relaxation rate depends on the wave vector of the electron as k^3 and, accordingly, significantly decreases with decreasing k . This allows us to immediately obtain an upper estimate for relaxation in the lower quantum confinement subband, replacing k with $\sqrt{2m^*(E_{e1} - E_{e0})/\hbar}$, we obtain $\left\langle \frac{dE(k)}{dt} \right\rangle_{\text{ZP}} < 1.4 \times 10^{11} \text{meV/s}$.

Appendix D. Interband recombination time

The characteristic time of radiative recombination of an electron and a hole in a quantum well can be calculated using an approach similar to that described in Refs. [16, 19]. The matrix element of the interband optical interaction contains the product of the overlap integral of the envelopes of the wave functions of the electron and the energy-split states of the heavy and light holes, $I_{(h,l)hNM} = \int \psi_{(h,l)hNM}^*(z) \psi_{eM}(z) dz \approx \delta_{NM}$ (the integral is small for transitions without preserving the state number), by the interband matrix element, the absolute values of which, together with the corresponding selection rules, are given in Ref. [16].

In order to obtain the lifetime of an electron with respect to the recombination process, it is necessary to sum the square of the matrix element with respect to all directions of propagation of an electromagnetic wave at two possible polarizations, taking into account the polarization selection rules. Neglecting small corrections, we obtain two contributions in the reverse recombination time, associated with recombination with heavy and light holes, respectively. Naturally, these contributions are proportional to the Fermi distribution function of heavy and light holes. Under the conditions of the proposed experiment, recombination with the participation of light holes can be neglected. Thus, the inverse time of radiative recombination with respect to interband transitions for the electronic subband N in the CGS system can be represented as follows:

$$\tau_N^{-1}(\mathbf{k}) = \frac{ne^2 E_p}{m_0 c^3 \hbar^2} [E_G + E_{eN}(\mathbf{k}) + E_{hhN}(\mathbf{k})] f_{hhN}(\mathbf{k}) \quad (\text{A.18})$$

where E_G is the band gap, E_p is the Kane matrix element, m_0 is the mass of a free electron, c is the speed of light, n is the refractive index, and $f_{hhN}(\mathbf{k})$ is the distribution function of heavy holes at the N level. Assuming $f_{hhN}(\mathbf{k}) \approx 1$, from Eq. (A.18) we can obtain an upper estimate for the inverse radiative recombination time of $2.8 \times 10^8 \text{s}^{-1}$ (the corresponding estimate for the radiative recombination time is 3.6 ns).

Appendix E. Intersubband optical transitions

The inverse time of the optical transition between subbands f and i in a quantum well can be calculated as follows [21]:

$$1/\tau_{fi}^{\text{opt}} = \frac{4e^2\omega_{fi}n}{c^3\hbar(m^*)^2} \left| (\hat{p}_z)_{fi} \right|^2 = \frac{16E_i E_f e^2 n \sin^2\left(\frac{1}{2}\pi(f+i)\right)}{c^3\hbar\omega_{fi}(m^*)^2(a/2+1/\kappa_i)(a/2+1/\kappa_f)} \quad (\text{A.19})$$

where \hat{p}_{fi} is the matrix element of the momentum operator, $\hbar\omega_{fi}$ is the optical transition energy. Calculations according to Eq. (A.19) give the value of the τ_{10}^{opt} time of the order of 9.2×10^{-7} s.

Appendix F. Shift of levels caused by Coulomb interaction

As we pointed out above, the relaxation rate of holes in the QW is significantly higher than the relaxation rate of electrons. We will assume that all of the holes are in the lower state of the QW. As for the electron subsystem, some of the electrons are at QC levels 1 and 2.

We will use the infinitely deep QW model for our estimation. In this model, the module squares of the wave functions of the electrons and holes in the ground state are the same. The charges of electrons and holes, for the most part, compensate each other.

The electrostatic potential $\phi(z)$ of the uncompensated charge can be expressed through the Poisson equation:

$$\frac{\partial^2\phi(z)}{\partial z^2} = -\frac{4\pi e}{\epsilon_0} \sum_{i=1}^2 n_i(t) \left[|\psi_i(z)|^2 - |\psi_0(z)|^2 \right]. \quad (\text{A.20})$$

Strictly speaking, the wave functions $\psi_i(z)$, in turn, depend on the potential, and Eq. (A.20) should be solved self-consistently, but for our evaluation, we will neglect this dependence. In this case, the equation is solved trivially:

$$\phi(z) = \frac{2ea}{\pi\epsilon_0} \left[n_1(t) \cos^4 \frac{\pi z}{2a} + \frac{n_2(t)}{2} \left(\cos \frac{\pi z}{a} - \frac{1}{9} \cos \frac{3\pi z}{a} \right) \right]. \quad (\text{A.21})$$

Then the first perturbation theory correction to the difference between the energies of excited states 1 and 2 will have the following form:

$$\delta E_{12} = \frac{Gae^2}{18\pi\epsilon_0} \left\{ \frac{1}{\gamma_{21}^{\text{PO}}} - \frac{5}{4\gamma_{21}^{\text{PO}}} \right\} \quad (\text{A.22})$$

The time dependence is missing here because we used the Eqs. (17) and (18) for a time longer than the transient time at the leading edge of the excitation pulse.

Estimation for reasonable pumping intensities gives us a correction of scale ≈ -0.1 meV

Appendix G. Shift of energy levels caused by exchange-correlation interaction

The exchange-correlation interaction can be taken into account in the plasmon pole approximation, as applied to the 2DEG system, see for example [18].

We are interested in the position of the QC level at a small longitudinal wavenumber so that we put the sample charge wavenumber at 0. This will increase the symmetry of the system and simplify the calculations. Then the energy shift of the bottom level j in the QW can be written [18] as:

$$\delta E_i(0) = -\frac{e^2}{\epsilon_0} \sum_{j=0}^2 \int_0^\infty f_j(q) \left\{ 1 - \frac{\hbar\omega_p^2}{2\omega_q \left[E_i - E_j - \frac{\hbar^2 q^2}{2m_e} + \hbar\omega_q \right]} \right\} dq. \quad (\text{A.23})$$

Plasma frequency in 2DEF systems is: $\omega_p = \sqrt{\frac{2\pi n(t)e^2 q}{\epsilon_0 \mu}} = \sqrt{\frac{2\pi G t e^2 q}{\epsilon_0 \mu}}$ and is assumed to depend only on the total concentration of nonequilibrium carriers, $\omega_q^2 = \omega_p^2 \left(1 + \frac{q}{\varkappa} + \frac{\hbar^2 q^4}{16\mu^2}\right)$ — effective plasma frequency, $\mu^{-1} = m_e^{-1} + m_{hh0}^{-1}$ — reduced electron-hole mass, $\varkappa = \frac{2e^2(m_e + m_{hh0})}{\epsilon_0 \hbar^2}$ — 2D screening wavenumber.

The formula (A.23) contains the sum over the transmitted wave vectors and finite states: $\delta E_i = \delta E_i^{(i)} + \delta E_i^{(o)}$. Let us first consider the contribution of electrons at the same level. For excited states of 1 and 2 the transmitted wave vector is small, so we can limit ourselves to the term with $j = i$ when the energy difference in the denominator turns to 0. Then Eq. (A.23) can be transformed to the form:

$$\delta E_2^{(i)} - \delta E_1^{(i)} = -\frac{e^2}{\epsilon_0} \int_{k_{F1}}^{k_{F2}} \left[1 - \frac{1}{2(1 - q/\varkappa)}\right] \approx -\frac{e^2}{4\epsilon_0 \gamma_{21}^{PO}} \sqrt{\pi G \gamma_{20}^{PO}} \approx -0.26 \text{ meV} \tag{A.24}$$

where the Fermi wave vector $k_{Fi} = \sqrt{2\pi n_i(t)}$, and the dependence $n_i(t)$ is given by in Eqs. (12) and (11).

For state 0 the situation is different — the electron distribution function $f_0(k, t)$ is maximal at $k = \sqrt{2m_e(E_1 - E_0)}$, at times $t < T$, where T is defined in the formula (10). The detailed form of the distribution function $f_0(k)$ can be established from Eq. (14).

$$\tilde{n}_0(t) = Gt = 2\pi \int_{k_{\min}(t)}^{k_{\max}} f_0(k) k dk \tag{A.25}$$

where $k_{\max} = \sqrt{2m_e(E_1 - E_0)}$, $k_{\min}(t) = k_{\max} - \left(\frac{dE}{dt}\right) \frac{m_e t}{\hbar^2 k_{\max}}$, where the energy relaxation rate is given by Eq. (A.16). For simplicity we replaced k by k_{\max} . Since $\left(\frac{dE}{dt}\right) \frac{1}{k} \propto k^2$, then such a substitution can only increase the area of integration and hence the magnitude of the correction.

By differentiating Eq. (A.25) over time, we can find the stationary distribution function:

$$f_0(k) = \frac{G \hbar^2}{m_e} \left(\frac{dE}{dt}\right)^{-1} < 0.02 \tag{A.26}$$

Then the shift between the QC levels of 1 and 2 can be written as:

$$\begin{aligned} \delta E_2^{(o)} - \delta E_1^{(o)} &= -\frac{e^2}{2\epsilon_0} \int_{k_{\min}(t)}^{k_{\max}} \frac{f_0(q) \hbar \omega_p^2}{\omega_q} \left\{ \frac{1}{E_1 - E_0 - \frac{\hbar^2 q^2}{2m_e} + \hbar \omega_q} - \frac{1}{E_2 - E_0 - \frac{\hbar^2 q^2}{2m_e} + \hbar \omega_q} \right\} dq \approx \\ &\approx \frac{e^2 \hbar \omega_p(k_{\max}) G t}{2\epsilon_0 (E_1 - E_0) k_{\max}} \end{aligned} \tag{A.27}$$

For $n(t) = Gt = 2 \times 10^{11} \text{ cm}^{-2}$ the exchange-correlation shift from this estimate is $\delta E_2^{(o)} - \delta E_1^{(o)} = 0.6 \text{ meV}$.

Acknowledgements A part of this work was carried out within the framework of the International Associated Laboratory PHYNICS.

Funding This work was partly supported by RFBR (#18-02-00002 and #20-52-16304).

References

1. M. Hangyo, Japanese Journal of Applied Physics **54** (2015), no. 12, 120101.
2. R. Köhler, A. Tredicucci, F. Beltram, H. E. Beere, E. H. Linfield, A. G. Davies, D. A. Ritchie, R. C. Iotti, and F. Rossi, Nature **417** (2002), no. 6885, 156.
3. B. S. Williams, Nature Photonics **1** (2007), no. 9, 517.
4. M.A. Belkin and F. Capasso, Physica Scripta **90** (2015), no. 11, 118002.
5. L.H. Li, L. Chen, J.R. Freeman, M. Salih, P. Dean, A.G. Davies, and E. H. Linfield, Electronics Letters **53** (2017), no. 12, 799.
6. O. Gauthier-Lafaye, P. Boucaud, F. H. Julien, S. Sauvage, S. Cabaret, J. M. Lourtioz, V. Thierry-Mieg, and R. Planel, Applied Physics Letters **71** (1997), no. 25, 3619.

7. O. Gauthier-Lafaye, F. H. Julien, S. Cabaret, J. M. Lourtioz, G. Strasser, E. Gornik, M. Helm, and P. Bois, *Applied Physics Letters* **74** (1999), no. 11, 1537.
8. S Adachi, *GaAs and Related Materials*. World Scientific, 1994.
9. K. Chang, *Phys. Rev. B* **61** (2000), 4743.
10. C. Weisbuch and B. Vinter, *Quantum Semiconductor Structures: Fundamentals and Applications*. Elsevier Science, 1991.
11. P. Sotirelis, P. von Allmen, and K. Hess, *Phys. Rev. B* **47** (1993), 12744.
12. L. E. Vorob'ev, *Journal of Experimental and Theoretical Physics Letters* **68** (1998), no. 5, 417.
13. B. K. Ridley, *Journal of Physics C: Solid State Physics* **15** (1982), no. 28, 5899.
14. B. K. Ridley, *Electrons and phonons in semiconductor multilayers*, 2nd ed., Cambridge University Press, Cambridge, 2009.
15. F. A. Riddoch and B. K. Ridley, *Journal of Physics C: Solid State Physics* **16** (1983), no. 36, 6971.
16. G. Bastard, *Wave Mechanics Applied to Semiconductor Heterostructures Monographies de physique*. Wiley, 1988.
17. C. Delalande, G. Bastard, J. Organasi, J. A. Brum, H. W. Liu, M. Voos, G. Weimann, and W. Schlapp, *Phys. Rev. Lett.* **59** (1987), 2690.
18. S. Schmitt-Rink and C. Ell, *Journal of Luminescence* **30** (1985), no. 1, 585.
19. B. K. Ridley, *Quantum processes in semiconductors*, 4th ed., Oxford University Press, USA, 2000.
20. V. F. Gantmakher and Y. B. Levinson, *Carrier scattering in metals and semiconductors*. Modern problems in condensed matter sciences 19 (North-Holland, 1987).
21. A. G. Petrov and A. Shik, *Physical Review B: Condensed Matter and Materials Physics* **48** (1993), no. 16, 11883.

Publisher's Note Springer Nature remains neutral with regard to jurisdictional claims in published maps and institutional affiliations.